Strong quantum fluctuations in a quantum spin liquid candidate with a Co-based triangular lattice

Ruidan Zhong[a], Shu Guo[a], Guangyong Xu[b], Zhijun Xu[b,c], and Robert J. Cava[a,1]

[a]Department of Chemistry, Princeton University, Princeton, NJ 08544; [b]National Institute of Standards and Technology Center for Neutron Research, National Institute of Standards and Technology, Gaithersburg, MD 20899; and [c]Department of Materials Science and Engineering, University of Maryland, College Park, MD 20742

Currently under active study in condensed matter physics, both theoretically and experimentally, are quantum spin liquid (QSL) states, in which no long-range magnetic ordering appears at low temperatures due to strong quantum fluctuations of the magnetic moments. The existing QSL candidates all have their intrinsic disadvantages, however, and solid evidence for quantum fluctuations is scarce. Here, we report a previously unreported compound, Na$_2$BaCo(PO$_4$)$_2$, a geometrically frustrated system with effective spin-1/2 local moments for Co^{2+} ions on an isotropic 2-dimensional (2D) triangular lattice. Magnetic susceptibility and neutron scattering experiments show no magnetic ordering down to 0.05 K. Thermodynamic measurements show that there is a tremendous amount of magnetic entropy present below 1 K in 0-applied magnetic field. The presence of localized low-energy spin fluctuations is revealed by inelastic neutron measurements. At low applied fields, these spin excitations are confined to low energy and contribute to the anomalously large specific heat. In larger applied fields, the system reverts to normal behavior as evident by both neutron and thermodynamic results. Our experimental characterization thus reveals that this material is an excellent candidate for the experimental realization of a QSL state.

quantum spin liquids | geometric frustrated magnets | quantum fluctuations | triangular lattice

A quantum spin liquid (QSL) is a unique type of spin liquid where strong quantum fluctuations prevent spins from ordering, which thus remain in a disordered liquid-like state even near absolute 0 (1, 2). Previous studies have shown that QSL states tend to emerge in low-spin geometrically frustrated systems, in which the interactions among the limited magnetic degrees of freedom are restricted by crystal geometry. This leads to a strong enhancement of quantum fluctuations (3). Several compounds with geometrically frustrated lattices have been proposed as QSL candidates (4–8). At present, the most widely accepted evidence for the QSL state is a broad continuous magnetic excitation observed in inelastic neutron scattering (INS) (6–8) believed to be associated with the fractionalized quasiparticles, spinons, that are expected for a QSL state (2). However, structural disorder and anisotropic spin interactions due to site mixing or lattice distortions in QSL candidates often result in a spin glass or magnetically ordered ground state, which can give rise to an impostor spin liquid-like state (9) and produce a broad continuum in INS (10). Unfortunately, the problem of site mixing or lattice distortion in the existing QSL candidates cannot be neglected (11–13). Similar fractionalized excitations have also been seen in Cs$_2$CuCl$_4$ (14) and Ba$_3$CoSb$_2$O$_9$ (15, 16), but those materials are known to have magnetically ordered states at low temperature (15, 17). Thus, all of the above materials evoke skepticism about whether the observation of a broad continuum feature in the INS can be uniquely attributed to the QSL state. Thus, when looking for a more robust characterization of the QSL state, a new ideal candidate with no disorder, isotropic magnetic exchange coupling, and a well-defined crystal structure is a necessary but challenging goal to pursue.

Here, we propose a QSL compound, Na$_2$BaCo(PO$_4$)$_2$, in which Co^{2+} with effective $S = 1/2$ resides on a geometrically frustrated triangular lattice. A significant advantage of this material is that it does not display any significant site mixing or lattice distortions—the magnetic Co^{2+} ions constitute isotropic triangular lattice layers with simple packing. Furthermore, single crystals can be grown. Direct current (dc) magnetic susceptibility and elastic neutron scattering experiments reveal no long-range magnetic ordering down to 0.3 K in the presence of antiferromagnetic interactions on the order of 32 K. In addition, alternating current (ac) magnetic susceptibility measured down to 0.05 K indicates no spin glass transition. The magnetic specific heat on a single crystal reveals the presence of a large magnetic entropy at low temperature. INS measurements indicate the presence of strong localized magnetic fluctuations, which are nearly temperature independent and have exotic behavior under a magnetic field. These observations indicate that this material is an excellent QSL candidate.

Results

Pink single crystals of Na$_2$BaCo(PO$_4$)$_2$ harvested from flux method growths have a layered morphology with hexagonal faces shown in Fig. 1*E*. Single-crystal X-ray diffraction data for Na$_2$BaCo(PO$_4$)$_2$ indicate a trigonal crystal structure, space group P $\bar{3}$ m1, with lattice constants of $a = b = 5.3185(1)$ Å and $c = 7.0081(1)$ Å. Detailed crystal data and crystal

Significance

The experimental search and verification of theoretically predicted quantum spin liquids (QSLs) are challenging, especially because there is no universally accepted evidence to support such exotic quantum states. At present, broad continuous magnetic excitations (i.e., a spinon continuum observed via inelastic neutron scattering) is considered as the most crucial evidence for a QSL as described in many studies on the existing QSL candidates. However, as another potential origin of such broad spin excitations, disorder effects in those candidates cannot be neglected. Here, we present a previously unreported compound with a Co-based triangular lattice that is structurally perfect and without intrinsic disorder. We present experimental results that suggest that this compound is an ideal QSL candidate for future studies.

Fig. 1. The crystal structure of $Na_2BaCo(PO_4)_2$. (*A*) The crystal structure for $Na_2BaCo(PO_4)_2$ based on the packing of M-O polyhedra. (*B*) The triangular layer of CoO_6 octahedra in the *ab* plane, with J_1 and J_2 marked to indicate the superexchange coupling between the nearest neighbor Co^{2+} ions in the same plane and the neighboring plane. (*C*) View emphasizing the layers of CoO_6 octahedra along the *c* axis viewed from the *b* axis. (*D*) Top view of the relative orientation of the CoO_6 and other groups in the 2D triangular layers. The lines in *C* and *D* indicate the unit cell. (*E*) Photo of the pink single crystals of $Na_2BaCo(PO_4)_2$.

structure refinement results are presented in Tables 1 and 2. A similar structure has been reported for several $Na_2BaM(VO_4)_2$ (M = Ni, Co, Mn, and Fe) compounds (18, 19), while the $Na_2BaCo(PO_4)_2$ compound studied here has not been previously reported. Because of the distinct difference in the constituent atoms' charge and ionic size, disorder due to the site mixing is a priori expected to be negligible as is shown to be the case in the structural refinements (Table 2). Furthermore, the single-crystal refinement indicates that the material is stoichiometric, with a simple whole number ratio of constituents. Schematic plots of the crystal structure are shown in Fig. 1*A*, *C*, and *D*. Triangular layers of magnetic CoO_6 octahedra are found in a simple A-A-A stacking pattern; the lattice disruptions due to stacking faults frequently seen in other hexagonal-layered geometrically frustrated magnets are not seen in this material, because there are no van der Waals-bonded planes present. The magnetic layers are instead separated by a single layer of nonmagnetic BaO_{12} polyhedra, with $[PO_4]^{3-}$ units and Na^+ filling the gaps in the cobalt oxide layers. Since Co is a $3d$ transition element, the magnetic exchange coupling strength depends on the overlap of metal–oxygen and oxygen–oxygen bonds (i.e., superexchange). As a result, the coupling between the nearest neighbor Co^{2+} ions in the same triangular layer (Fig. 1*B*, J_1) is through a Co-O-O-Co super-superexchange path, while the exchange coupling with Co^{2+} ions in the neighboring layers (J_2) is through Co-O-O-O-Co super-super-superexchange. Therefore, despite the fact that the Co-Co spacing between interlayers (7.00 Å) and intralayer (5.32 Å) is moderately close, this is deceptive. J_2, the coupling between planes, should be much smaller than J_1, the in-plane exchange, due to the weaker exchange path. Therefore, the system can be considered as an effectively 2-dimensional (2D) triangular magnet and thus, may show the effects of strong geometrical frustration.

Fig. 2*A* shows the *dc* magnetic susceptibility of $Na_2BaCo(PO_4)_2$ down to 1.8 K. In contrast to the analogous materials $Na_2BaCo(VO_4)_2$ and $Na_2BaNi(VO_4)_2$, which have ordering transitions at 3.9 and 8.4 K, respectively (19), no magnetic phase transition is observed for $Na_2BaCo(PO_4)_2$.

Since Co^{2+} is a Kramers ion, the effective magnetic moment of Co^{2+} can be regarded as $S = 1/2$ (20, 21), similar to what is observed in isostructural $Na_2BaCo(VO_4)_2$ (19). The Curie–Weiss law was applied to fit the susceptibility from 200 to 300 K without including a Pauli susceptibility χ_0. From the fits, we find $\Theta_{CW,\perp} = -31.9$ K, $\mu_{eff,\perp} = 4.96$ μ_B and $\Theta_{CW,\parallel} = -32.6$ K, $\mu_{eff,\parallel} = 5.87$ μ_B for the magnetic field applied perpendicular and parallel to the c axis, respectively, indicating that the antiferromagnetic interactions dominate. The large effective moment suggests a nonnegligible orbital contribution to the magnetic moment. Using these fitted Θ_{CW} values, we estimate the exchange interaction constant J/k_B to be 21.4 K (10, 22). Despite the expected difference in the exchange coupling based on the crystal structure, the magnetic anisotropy is significant but not large, further confirmed by the field-dependent magnetization shown in Fig. 2*A*, *Inset*. Due to the nearly isotropic

Table 1. Crystal data and ambient temperature crystal structure refinements for $Na_2BaCo(PO_4)_2$

Formula	$Na_2BaCo(PO_4)_2$
Formula mass (g/mol)	432.21
Crystal system	Trigonal
Space group, Z	P$\bar{3}$m1 (no. 164), 1
a (Å)	5.3185(1)
c (Å)	7.0081(1)
V (Å^3)	171.676(5)
T (K)	298 (2)
ρ (cal) (g/cm^3)	4.180
λ (Å)	0.71073
F (000)	199
θ (°)	2.91–33.14
Crystal size (mm^3)	$0.065 \times 0.065 \times 0.04$
μ (mm^{-1})	8.721
Final R indices	$R_1 = 0.0260, \omega R_2 = 0.0574$
R indices (all data)	$R_1 = 0.0272, \omega R_2 = 0.0580$
Goodness of fit	1.197

Table 2. Wyckoff positions, coordinates, occupancies, and equivalent isotropic displacement parameters for $Na_2BaCo(PO_4)_2$

Atom	Wyckoff site	x	y	z	Occupancy	U_{eq}
Ba_1	1a	0	0	0	1	0.01031 (18)
Co_1	1b	0	0	0.5	1	0.0069 (3)
P_1	2d	0.3333	0.6667	0.2420 (3)	1	0.0064 (4)
Na_1	2d	0.3333	0.6667	0.6794 (6)	1	0.0162 (8)
O_2	2d	0.3333	0.6667	0.0250 (8)	1	0.0128 (12)
O_1	6i	0.1793 (5)	0.8207 (5)	0.3188 (6)	1	0.0417 (14)

magnetization in response to field, the sample orientation under field is only a minor factor in the subsequent physical measurements.

Neutron powder diffraction data obtained at 0.3 and 10 K provide more information about the magnetic characterization of the compound. From the above dc susceptibility results, the system is far from ordering at 10 K. By comparing the neutron diffraction peaks measured at both temperatures (Fig. 2B), we find no extra superlattice peaks in the 0.3 K pattern compared with the one measured at higher temperature, and the intensities differ only within error. The magnetic peaks associated with long-range magnetic ordering should be strong at small Q due to the magnetic form factor. Thus, the blownup view shown in Fig. 2B, Inset further indicates there is no magnetic ordering (15) down to 0.3 K. No frequency dependence in the ac magnetic susceptibility is found down to 50 mK as shown in Fig. 2C, indicating that there is no spin freezing present. The nature of the frequency-independent hump around 0.35 K is not clear, but a similar feature found in the Co-based material $Na_3Co(CO_3)_2Cl$ at 17 K has not been attributed to either a magnetic ordering or a spin glass transition (23).

In Fig. 3A, we present the specific heat C_p down to 0.35 K for a $Na_2BaCo(PO_4)_2$ single crystal. Under 0 field, neither a peak, as would be expected for a well-defined magnetic phase transition, nor a broad hump, as would be typical for a spin glass system (10, 13, 24), are observed, consistent with all of our other data. For applied field above 3 T, there is still no evidence of long-range magnetic ordering, but instead, a broad peak appears. This broad hump is associated with Schottky anomaly that shifts to higher temperatures at higher fields.

A dramatic transition in behavior is found at a critical field, denoted as H*, around 2~3 T. A single crystal of the nonmagnetic isostructural analogue $Na_2BaMg(PO_4)_2$ was used for subtraction of phonon contribution to the total heat capacity, allowing us to calculate the magnetic specific heat Cm for $Na_2BaCo(PO_4)_2$ as shown in Fig. 3B. The upturning feature that appears at the lowest temperatures in C_m/T for $Na_2BaCo(PO_4)_2$ is unexpected. A similar upturning feature found in some materials (4, 25, 26) has been attributed to a nuclear Schottky contribution arising from the nuclei of the constituent atoms. In our case, however, we rule out this possibility by separately measuring the specific heats of the related materials $Na_2BaMg(PO_4)_2$ (Fig. 3C) and $BaCo_2As_2O_8$ down to 0.35 K (Fig. 3D). These materials contain all of the atoms (and their nuclei) that are present in $Na_2BaCo(PO_4)_2$ but do not show this feature in the studied temperature range. In addition, the magnitude of the measured magnetic specific heat for $Na_2BaCo(PO_4)_2$ in this temperature range is several orders of magnitude larger than that of a nuclear Schottky contribution (4, 25, 26), which further indicates that there is a tremendous amount of magnetic entropy present at low temperatures in this material. To determine the magnetic entropy ΔS_m, we first interpolated the curve of C_m/T vs. T to 0 K and then performed

the integration. Due to the upturning feature at the lowest temperature, the integration for magnetic entropy is not complete. In fact, for a $S = 1/2$ QSL system, the expected total magnetic entropy should reach to exactly $Rln2$ (R = the ideal gas constant). Nevertheless, the obtained magnetic entropy for 0 field reaches only $0.71Rln2$ by 30 K. The difference between this value and $Rln2$ indicates that more magnetic entropy is present below 0.3 K. By applying a field larger than 4 T, conventional thermodynamic behavior returns, giving rise to a total entropy that is precisely $Rln2$ (in Fig. 3B, Inset, selected fields are presented for clarity).

Characteristic signatures for strong quantum fluctuations are observed in INS measurements on the powder sample. Lowenergy (1-meV) scattering intensities measured with or without an applied magnetic field at 10 K are shown in Fig. 4A. We see similar intensities over the Q range that we measured, and the magnetic excitation intensities show no significant Q dependence. Having a relatively flat Q dependence implies that these intensities are related to fluctuations localized in real space, possibly due to strong frustration in the system. While these intensities do respond to an external magnetic field, it is evident that these are indeed localized spin fluctuations.

We now focus on the temperature and field dependence of the magnetic excitations seen by quasielastic neutron scattering at an arbitrary position in scattering space, $Q = 1.276 \text{ Å}^{-1}$, corresponding to $(H, K, L) = (1/3, 2/3, 0)$ in reciprocal space. Fig. 4B shows the energy dependence of the scattering intensity obtained at temperatures ranging from 0.3 to 10 K. The overall shape and intensity do not change much with temperature, indicating that the low-energy spin fluctuations are not much affected by temperature up to 10 K. This observation coincides with that of $\alpha - RuCl_3$ (27), which shows that an insignificantly affected intensity at higher temperature for the higher-energy mode accounted for proximate Kitaev QSL state. Moreover, one can see that the "quasielastic" peak is not actually symmetric about $\hbar\omega = 0$. The degree of asymmetry slightly decreases when heating to 10 K as shown in the zoomed-in plots in Fig. 4C, which indicates that the spin fluctuations slightly shift to slightly lower energy. The measured spectra, indicated by the dashed lines in Fig. 4B, can be fit as a sum of incoherent elastic scattering (black line in Fig. 4B) and a quasielastic spin excitation (colored lines in Fig. 4B). After subtraction of the incoherent scattering, one can determine a low-energy magnetic excitation (solid colored lines in Fig. 4B) with energy scale 0.18 to 0.2 meV.

The energy resolution of the SPINS instrument is not enough to cleanly separate the inelastic magnetic excitations from the elastic background. Nonetheless, the magnetic field response of these low-energy spin excitations at both 0.3 and 10 K reflects the inelastic nature of the scattering. At 0.3 K (Fig. 4D), the spectrum is dominated by excitations from the ground state to the excited state, and thus, we only see intensities on the neutron energy loss side (positive energy side); while at 10 K (Fig. 4E), the excited state becomes populated, and the spectrum also includes
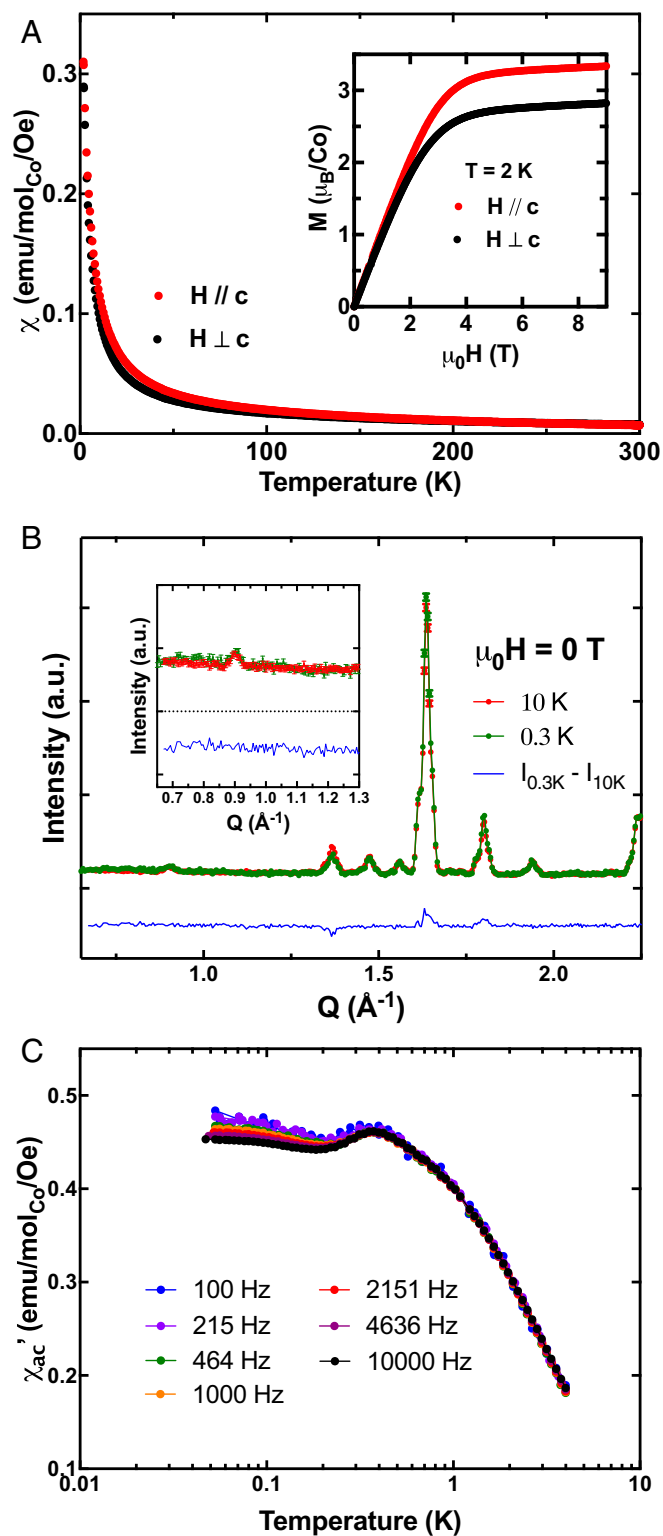
Fig. 2. No long-range or glassy magnetic ordering is observed in Na$_2$BaCo(PO$_4$)$_2$ down to 0.05 K. (*A*) Temperature dependence of the *dc* susceptibility down to 1.8 K measured with μ_0H = 0.1 T on a single crystal sample oriented with the external field perpendicular to the *c* axis ($H \perp c$; black) and parallel to the *c* axis ($H \parallel c$; red). (*Inset*) Field dependence of magnetization measured in both crystal orientations. (*B*) Neutron powder diffraction pattern for Na$_2$BaCo(PO$_4$)$_2$ measured at 0.3 K (green) and 10 K (red) as well as their difference (blue). (*Inset*) Zoomed-in view of neutron diffraction pattern showing the low-Q region. (*C*) Temperature dependence of the real part of the *ac* magnetic susceptibility measured down to 0.05 K.

intensities coming from the energy gain side (negative energy side). The relative intensities follow the detailed balance principle $S(Q, -\hbar\omega) = e^{-\hbar\omega/k_BT}S(Q, \hbar\omega)$. The splitting observed at high field is likely of a conventional Zeeman type. Note that, at higher fields in both temperatures, when the quasielastic spin excitation peak shifts away from the elastic background to higher energy, the remaining elastic feature (black lines in Fig. 4 *D* and *E*) becomes symmetric around 0. This further indicates that the asymmetric peaks observed at low fields are indeed due to extra magnetic components on the positive energy side. The energy needed to excite such magnetic states at different fields can be extracted from the fitted peak center as plotted in Fig. 4*F*. At a field smaller than H* (μ_0H = 0T, 2T), the excitation energy is small and relatively constant, seeming to indicate a constant energy gap between the ground state and the spin excitation continuum. In contrast to the field response of the spin wave excitations in a conventional magnet, the preserved spin excitations observed here further suggest that we have an unconventional magnetic system. In support of this, the unaffected spinon excitations under weak field have been discussed in earlier reports both experimentally (28) and theoretically (29). With a strong field larger than H* (μ_0H = 4T, 6T), the magnetic excitations are now peaked at higher energies, clearly separated from the incoherent elastic peak, and the excitation energy increases linearly with field. The linear relation in the high field regime seems to indicate a conventional Zeeman splitting behavior of magnon excitations and agrees with the expectation for the nearly polarized magnetic state.

Interestingly, the exotic nonlinear field response agrees well with the specific heat measurements. At fields less than H*, one still observes a non-0 specific heat response at the lowest temperature. It is reasonable to expect that, with no applied magnetic field or small field, the quantum spin fluctuations are "forced" into the low energy (<0.2 meV) channels and therefore, contribute to the anomalous specific heat in this QSL. Only with large field when the conventional Zeeman splitting behavior dominates, these spin excitations can be shifted to higher energies, and the specific heat of the system reverts back to normal behavior.

From the energy-integrated intensity of the spin excitations seen in the neutron scattering data, one can perform an absolute normalization to determine the size of spin fluctuations (30). The calculated fluctuating moment is then $m = g\sqrt{S(S+1)} = 1.52\mu_B/\text{Co}^{2+}$, indicating strong magnetic fluctuations compared with the total local moment. This also provides an independent estimation of the effective magnetic moment $S = 1/2$. We note that the integrated intensities of spin excitations at different temperatures and fields are comparable, indicating that most of the spin fluctuation spectral weight is confined to low energy and shifts to higher energies at sufficiently high applied field.

Conclusions

Our observations on the compound Na$_2$BaCo(PO$_4$)$_2$ reveal its potential as a previously unreported quantum spin liquid candidate. No magnetic ordering or spin freezing is observed down to 0.05 K. Thermodynamic measurements show that there is tremendous magnetic entropy present below 1 K, a reflection of the presence of a very large spin density of states at low temperatures. INS measurements show a flat Q dependence for the low-energy magnetic excitations, corresponding to localized low-energy spin fluctuations, which are persistent with changing temperature and weak magnetic field. The exotic temperature and magnetic field response of these low-energy magnetic excitations further indicates the nontrivial nature of the magnetic ground state of Na$_2$BaCo(PO$_4$)$_2$. Since this discovered compound is structurally superior to the other existing QSL candidates, any

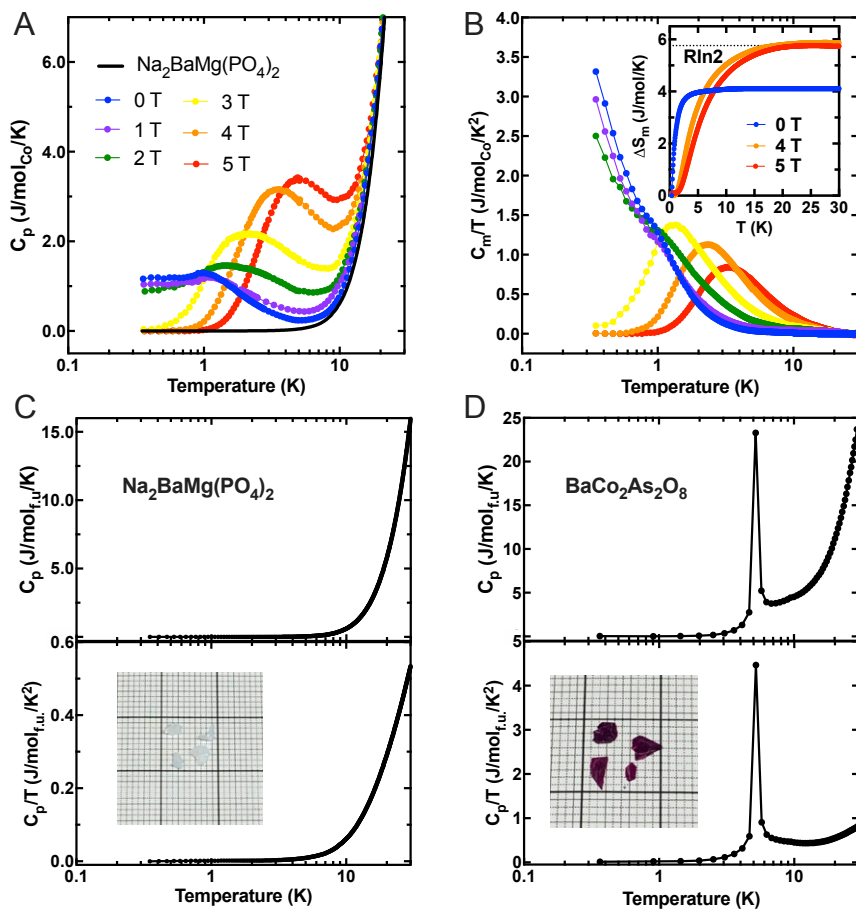**Fig. 3.** Magnetic specific heat results for $Na_2BaCo(PO_4)_2$. (*A*) Heat capacity C_p as a function of temperature for a $Na_2BaCo(PO_4)_2$ single crystal measured under several applied magnetic fields. (*B*) C_m/T as a function of temperature at several magnetic fields. (*Inset*) Temperature dependences of integral magnetic entropy under magnetic fields of 0, 4, and 5 T for $Na_2BaCo(PO_4)_2$. (*C* and *D*) Heat capacities for $Na_2BaMg(PO_4)_2$ and $BaCo_2As_2O_8$, respectively, measured in the same temperature range.

broad continuum excitation found in future inelastic neutron experiments could be associated with the spinons, which are a consequence of the QSL state, instead of disorder.

Materials and Methods

Materials Synthesis. Single crystals of $Na_2BaCo(PO_4)_2$ for *dc* susceptibility, specific heat, and thermal conductivity measurements were synthesized by the flux method. Dried Na_2CO_3 (99%; Alfa Aesar), $BaCO_3$ (99.95%; Alfa

Aesar), CoO (99%; Alfa Aesar), and $(NH_4)_2HPO_4$ (99.5%; Sigma-Aldrich) were mixed stoichiometrically and ground well with the flux media NaCl in a molar ratio of 1:5. The mixed starting materials were loaded in an alumina crucible and then heated up to 950 °C for 2 h followed by a slow cooling procedure of 3 °C/h to 750 °C. The obtained pink single crystals were manually separated from the bulk. Polycrystalline $Na_2BaCo(PO_4)_2$ samples for *ac* susceptibility and neutron scattering were prepared by a solid-state reaction: a stoichiometric mixture of the above starting materials was ground
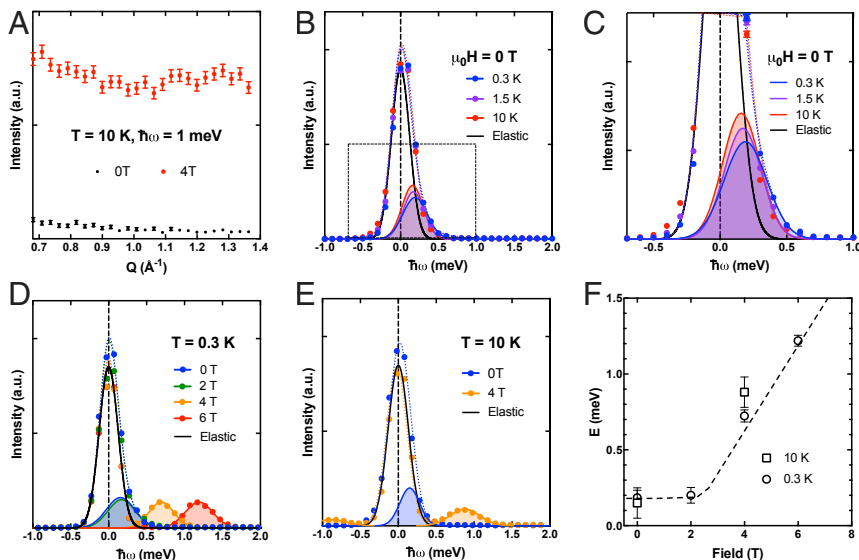

Fig. 4. Evidence for strong quantum fluctuations in $Na_2BaCo(PO_4)_2$. (*A*) INS intensity ($\hbar\omega = 1$ meV) as a function of wave vector Q under magnetic fields of 0 and 4 T measured at 10 K. (*B*) Zero-field quasielastic neutron scattering spectra measured at 0.3, 1.5, and 10 K, respectively. The dotted box in *B* is expanded in *C*. (*C*) Detailed view of the neutron scattering spectra showing the asymmetric characteristics at all temperatures. (*D* and *E*) Energy dependence of the scattering for $Na_2BaCo(PO_4)_2$ with applied magnetic fields measured at 0.3 and 10 K, respectively. In *B*–*E*, dots are experimental data, the dashed lines are the fits described in the text, the black curves indicate the fits to the incoherent elastic scattering, and the colored solid lines as well as their shaded areas show the contribution from spin fluctuations under different conditions. (*F*) Energy of characteristic magnetic excitations under applied magnetic fields ranging from 0 to 6 T. The dashed line in *F* is a guide to the eyes.

together with a catalyst NH_4Cl (1:0.5 in molar ration) and sintered in air in stages to 700 °C for 24 h.

Single-Crystal X-Ray Diffraction Measurements and Refinements. The crystal structure was determined by single-crystal X-ray diffraction. The diffraction data were collected at 298(2) K with a Kappa Apex2 CCD diffractometer (Bruker) using graphite-monochromated Mo-Kα radiation (λ = 0.71073 Å). The raw data were corrected for background, polarization, and the Lorentz factor, and multiscan absorption corrections were applied. Finally, the structure was analyzed by the Intrinsic Phasing method provided by the ShelXL structure solution program (31) and refined using the ShelXL least squares refinement package with the Olex2 program (32, 33).

Magnetization and Thermodynamic Measurements. The *dc* magnetic susceptibility was measured in a physical property measurement system (PPMS) that cooled to 1.8 K (PPMS-DynaCool; Quantum Design). The *ac* susceptibility measurements on a polycrystalline pellet sample were conducted in a Quantum Design PPMS DynaCool with a dilution refrigerator insert (ACDR measurement option) allowing for a measurement down to 0.05 K. Specific heat was measured in a PPMS equipped with a ^{3}He inset. All heat capacity measurements were carried out with external magnetic field applied parallel to the *c* axis of a single crystal.

Neutron Scattering Measurements. Elastic neutron scattering and INS experiments were performed on the NG5-Spin Polarized Inelastic Neutron Spectrometer, a cold neutron source located at the National Institute of Standards and Technology Center for Neutron Research. The 25-g powder sample was tightly packed into an aluminum sample holder, which was then mounted in a closed-cycle refrigerator equipped with a ^{3}He insert for cooling. We held the system at the base temperature overnight to guarantee a homogeneous temperature of our powder sample. The collimators used for this experiment were Guide-80-80-open, with a fixed incident energy of 5 meV (λ = 4.045 Å). Energy resolution was about 0.3 meV under current settings. The wave vector Q is expressed as $|Q| = 2|k_i| sin2\theta$, where 2θ is the angle between the incident and the final beam.

Data Availability. The physical property and neutron scattering datasets generated during and/or analyzed during this study are available from the corresponding author on request.

1. F. Mila, Quantum spin liquids. *Eur. J. Phys.* **21**, 499–510 (2000).
2. L. Balents, Spin liquids in frustrated magnets. *Nat. Mater.* **464**, 199–208 (2010).
3. R. Moessner, A. P. Ramirez, Geometrical frustration. *Phys. Today* **59**, 24–29 (2006).
4. S. Yamashita et al., Thermodynamic properties of a spin-1/2 spin liquid state in a κ-type organic salt. *Nat. Phys.* **4**, 459–462 (2008).
5. M. Yamashita et al., Highly mobile gapless excitations in a two-dimensional candidate quantum spin liquid. *Science* **328**, 1246–1248 (2010).
6. T.-H. Han et al., Fractionalized excitations in the spin-liquid state of a kagome-lattice antiferromagnet. *Nature* **492**, 406–410 (2012).
7. Y. Shen et al., Evidence for a spinon Fermi surface in a triangular lattice quantum-spin-liquid candidate. *Nature* **540**, 559–562 (2016).
8. J. A. M. Paddison et al., Continuous excitations of the triangular-lattice quantum spin liquid YbMgGaO$_4$. *Nat. Phys.* **13**, 117–122 (2017).
9. Z. Zhu et al., Disorder-induced mimicry of a spin liquid in YbMgGaO$_4$. *Phys. Rev. Lett.* **119**, 157201 (2017).
10. Z. Ma et al., Spin-glass ground state in a triangular-lattice compound YbZnGaO$_4$. *Phys. Rev. Lett.* **120**, 087201 (2018).
11. D. E. Freedman et al., Site specific X-ray anomalous dispersion of the geometrically frustrated Kagome magnet, Herbertsmithite, ZnCu$_3$ (OH)$_6$Cl$_2$. *J. Am. Chem. Soc.* **132**, 16185 (2010).
12. T. Han, S. Chu, Y. S. Lee, Refining the spin Hamiltonian in the spin-1/2 Kagome lattice antiferromagnet ZnCu$_3$ (OH)$_6$Cl$_2$ using single crystals. *Phys. Rev. Lett.* **108**, 157202 (2012).
13. Y. Li et al., Gapless quantum spin liquid ground state in the two-dimensional spin-1/2 triangular antiferromagnet YbMgGaO$_4$. *Sci. Rep.* **5**, 16419 (2015).
14. R. Coldea et al., Z. Experimental realization of a 2D fractional quantum spin liquid. *Phys. Rev. Lett.* **86**, 1335–1338 (2001).
15. H. D. Zhou et al., Successive phase transitions and extended spin-excitation continuum in the *S* = 1/2 triangular-lattice antiferromagnet Ba$_3$CoSb$_2$O$_9$. *Phys. Rev. Lett.* **109**, 267206 (2012).
16. S. Ito et al., Structure of the magnetic excitations in the spin-1/2 triangular-lattice Heisenberg antiferromagnet Ba$_3$CoSb$_2$O$_9$. *Nat. Comm.* **8**, 234 (2017).
17. R. Coldea et al., Neutron scattering study of the magnetic structure of Cs$_2$CuCl$_4$. *J. Phys Condens. Matter* **8**, 7473 (1996).
18. A. Reuß et al., Screw-type motion and its impact on cooperativity in BaNa$_2$ Fe[VO$_4$]$_2$. *Inorg. Chem.* **57**, 6300–6308 (2018).
19. G. Nakayama et al., Synthesis and magnetic properties of a new series of triangular-lattice magnets, Na$_2$Ba*M*V$_2$O$_2$ (*M*=Ni, Co, and Mn). *J. Phys. Condens. Matter* **25**, 116003 (2013).
20. Y. Shirata et al., Experimental realization of a spin-1/2 triangular-lattice Heisenberg antiferromagnet. *Phys. Rev. Lett.* **108**, 057205 (2012).
21. M. E. Lines, Magnetic Properties of CoCl$_2$ and NiCl$_2$. *Phys. Rev.* **131**, 546–555 (1963).
22. Y. Li et al., Rare-earth triangular lattice spin liquid: A single-crystal study of YbMgGaO$_4$. *Phys. Rev. Lett.* **115**, 167203 (2015).
23. Z. Fu et al., Coexistence of magnetic order and spin-glass-like phase in the pyrochlore antiferromagnet Na$_2$Co(CO$_3$)$_2$Cl. *Phys. Rev. B* **87**, 214406(2013).
24. R. Zhong et al., Field-induced spin-liquid-like state in a magnetic honeycomb lattice. *Phys. Rev. B* **98**, 220407 (2018).
25. H. K. Collan, M. Krusius, G. R. Pickett, Specific heat of antimony and bismuth between 0.03 and 0.8 K. *Phys. Rev. B* **1**, 2888–2895 (1970).
26. S. Yamashita et al., Gapless spin liquid of an organic triangular compound evidenced by thermodynamic measurements. *Nat. Comm.* **2**, 275 (2011).
27. A. Banerjee et al., Proximate Kitaev quantum spin liquid behavior in a honeycomb magnet. *Nat. Mater.* **15**, 733 (2016).
28. Y. Shen et al., Fractionalized excitations in the partially magnetized spin liquid candidate YbMgGaO$_4$. *Nat. Comm.* **9**, 4138 (2018).
29. Y. D. Li, G. Chen, Detecting spin fractionalization in a spinon Fermi surface spin liquid. *Phys. Rev. B* **96**, 075105 (2017).
30. G. Xu, Z. Xu, J. M. Tranquada, Absolute cross-section normalization of magnetic neutron scattering data. *Rev. Sci. Instrum.* **84**, 083906 (2013).
31. G. M. Sheldrick, Crystal structure refinement with SHELXL. *Acta Crystallogr. Section C. Struct. Chem.* **71**, 3–8 (2015).
32. O. V. Dolomanov et al., OLEX2: A complete structure solution, refinement and analysis program. *J. Appl. Crystallogr.* **42**, 339–341 (2009).
33. A. L. J. Spek, Single-crystal structure validation with the program PLATON. *J. Appl. Crystallogr.* **36**, 7–13 (2003).